Smart Structures and Systems, *Vol. 25, No. 5 (2020) 593-604*
DOI: https://doi.org/10.12989/sss.2020.25.5.593

Temperature distribution analysis of steel box-girder based on long-term monitoring data

Hao Wang*[1], Qingxin Zhu [1a], Zhongqin Zou [1], Chenxi Xing [2], Dongming Feng [3] and Tianyou Tao [1]

[1] *Key Laboratory of C&PC Structures of Ministry of Education, Southeast University, Nanjing, China*
[2] *School of Law, Southeast University, Nanjing, China*
[3] *Weidlinger Transportation Practice, Thornton Tomasetti, New York, USA*

(*Received August 24, 2019, Revised November 20, 2019, Accepted December 9, 2019*)

Abstract. Temperature may have more significant influences on structural responses than operational loads or structural damage. Therefore, a comprehensive understanding of temperature distributions has great significance for proper design and maintenance of bridges. In this study, the temperature distribution of the steel box girder is systematically investigated based on the structural health monitoring system (SHMS) of the Sutong Cable-stayed Bridge. Specifically, the characteristics of the temperature and temperature difference between different measurement points are studied based on field temperature measurements. Accordingly, the probability density distributions of the temperature and temperature difference are calculated statistically, which are further described by the general formulas. The results indicate that: (1) the temperature and temperature difference exhibit distinct seasonal characteristics and strong periodicity, and the temperature and temperature difference among different measurement points are strongly correlated, respectively; (2) the probability density of the temperature difference distribution presents strong non-Gaussian characteristics; (3) the probability density function of temperature can be described by the weighted sum of four Normal distributions. Meanwhile, the temperature difference can be described by the weighted sum of Weibull distribution and Normal distribution.

Keywords: temperature distribution; steel-box girder; filed monitoring data; cable-stayed bridge; temperature difference; probability density

1. Introduction

Bridges are inevitably affected by the daily, seasonal, and annual air temperature variations. The corresponding temperature-induced deformation and stress during operation are often comparable to that due to operational loads and structural damages (Ho and Liu 1989, Saetta *et al*. 1995, Tong *et al*. 2001, Xia *et al*. 2011, 2017), which will cause longitudinal expansion and contraction of the bridge as well as bending on the vertical plane. Large forces that may cause further structural damages are thus easily developed at the bearings and the conjunction of expansion joints due to their restriction to span movements (Guo *et al*. 2014, Zhang *et al*. 2015). With the increase of bridge span length, the sensitivity to temperature also significantly increases. In some recent experimental and numerical studies, thermal effects on long-span bridges have been proved to be more significant than that of vehicle loads (Salawu 1997, Xu *et al*. 2010). Therefore, temperature effect is one of the most important factors that affect the mechanical properties of long-span bridges.

With the development of the structural health monitoring system (SHMS), field monitoring of temperature and the temperature effect has recently been carried out on some bridges (Macdonald and Daniell 2005). Many pioneering work on the temperature-induced response has been conducted. For example, Zuk (1965) investigated the thermal behavior of several highway bridges and found that their temperature distribution was affected by air temperature, wind, humidity, intensity of solar radiation, and material type. Ye *et al*. (2009) observed the Beijing-Hangzhou Grand Canal Bridge and obtained the vertical temperature distribution model for the pre-stressed concrete box girder. Im and Chang (2004) monitored and analyzed a 6-span steel and concrete composite box in Seoul. It was found that the transverse temperature difference existed in the box girder, which was about 50% of the vertical temperature difference. Xia *et al*. (2013) conducted a health monitoring study on the Tsing Ma Bridge, and found that the vertical displacements of the deck sections and cable sections at the main span are well correlated with the effective deck temperature. Zhou *et al*. (2012) analyzed the monitoring temperature data of the flat steel box girder of the Runyang Yangtze River Bridge and proposed a probability distribution model for the temperature difference among the measurement points. The temperature difference model of the girder is thus summarized. However, studies on the temperature distribution of flat steel-box girders of long-span bridges are still insufficient. Therefore, more studies need to be conducted to characterize the temperature distribution characteristics of the flat steel-box girder (Yarnold and Moon 2015).

*Corresponding author, Professor,
E-mail: wanghao1980@seu.edu.cn
[a] Ph.D. Student, E-mail: xinzqx@163.com

http://www.techno-press.org/?journal=sss&subpage=7
ISSN: 1738-1584 (Print), 1738-1991 (Online)

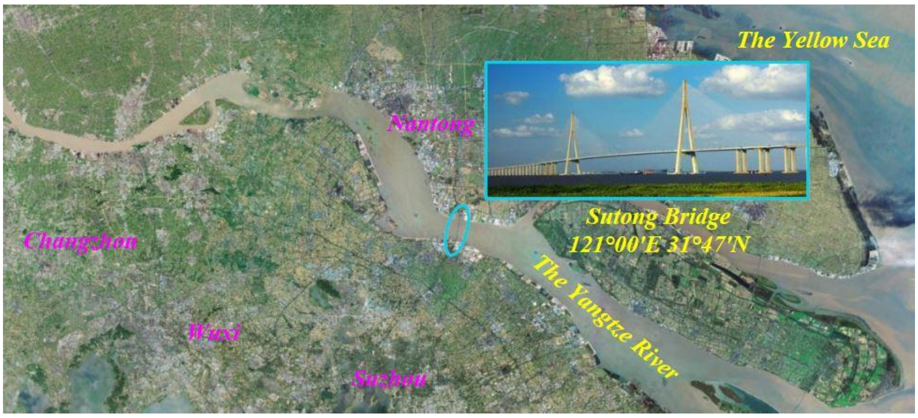

Fig. 1 The SCB

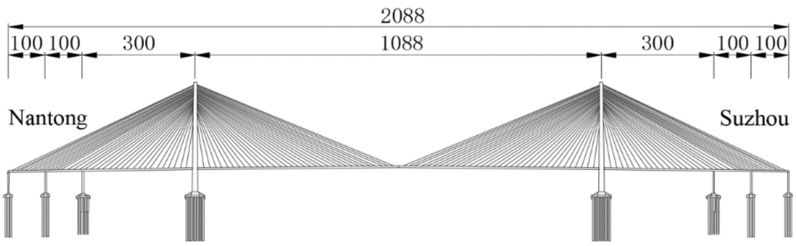

Fig. 2 Structural Layout of the SCB (Unit: m)

In this study, the temperature distribution of the steel box girder is systematically investigated based on the field monitoring data. Firstly, the Sutong Cable-stayed Bridge (SCB) and its SHMS are introduced. Secondly, the characteristics of temperature and temperature difference are examined based on one-year monitoring data. Thirdly, the probability density distributions of the temperature and temperature difference are calculated. Accordingly, the general formulas are proposed to describe the probability density distributions of the temperature and temperature difference. In addition, the effectiveness of the provided formulas is verified using field measurements.

2. Description of the SCB

In this study, the temperature distribution characteristics of the flat steel-box girder are investigated based on the long-term monitoring data recorded on the SCB. The SCB, connecting Nantong and Suzhou (as shown in Fig. 1), is a long-span cable-stayed bridge across the Yangtze River in Jiangsu Province. The bridge has a main span of 1088 m and double 500 m side spans (Fig. 2). Two 306-meter-tall inverted Y-shaped reinforced concrete bridge towers support the bridge deck with 272 symmetrically distributed cables (Zhang *et al*. 2009).

To ensure the safety, durability, and serviceability of the SCB under long-term heavy traffic loads, a comprehensive SHMS has been installed on the bridge since its opening to traffic in 2008. The system can reveal valuable information from the field measurements and assess the structural health status in real time (Spencer *et al*. 2004). The layout of temperature sensors on the flat steel box girder section is shown in Fig. 3. There are 18 temperature measurement points, numbered from T1 to T18. T1, T2, T3 and T4 are mounted on the top of the box girder (referred to as "upper plate" points) to monitor the temperature below the asphalt layer of pavement. T5, T6, T7 and T8 are mounted on the bottom of the upper U ribs of the box girder ("upper U rib" points) to monitor the temperature inside the steel box

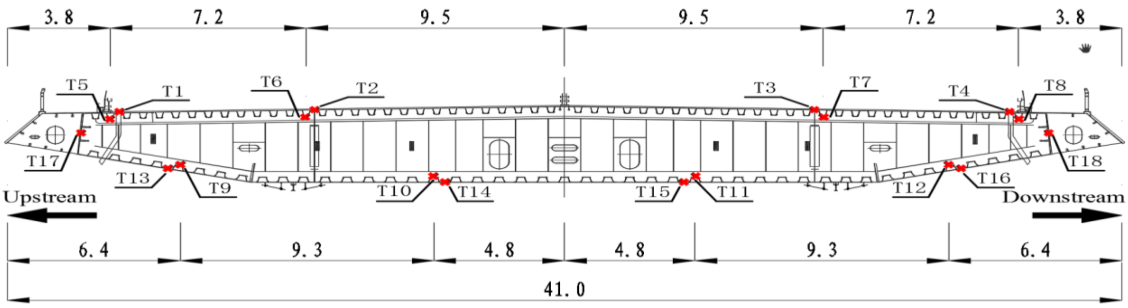

Fig. 3 Layout of temperature sensors (Unit: m)

girder roof. T9, T10, T11 and T12 are mounted on the top of the bottom U ribs (“bottom U rib” points) to monitor the temperature inside the box girder floor. T13, T14, T15 and T16 are mounted on the bottom of the box girder bottom plate (“bottom plate” points) to monitor the temperature outside the bottom plate. All the measurement points are symmetrically arranged about the centerline of the cross section. During the measurement, the sampling frequencies of all the sensors are set to 10 Hz (Wang *et al*. 2016). The temperature variation is small in a short time interval. Hence, the mean value during 5 minutes is used to investigate the temperature distribution.

3. Temperature distribution of the SCB

Based on the one-year field monitoring data of the SCB, the analysis on the monitoring temperature data of the mid-span section of the main girder is conducted. The temperature measurement at each point and the temperature difference between two adjacent points are analyzed based on the least-squares estimation and the hypothesis test. Fig. 4 presents the temperature variations of the flat steel-box girder. The raw data were recorded from January 1st, 2010 to December 31st, 2010.

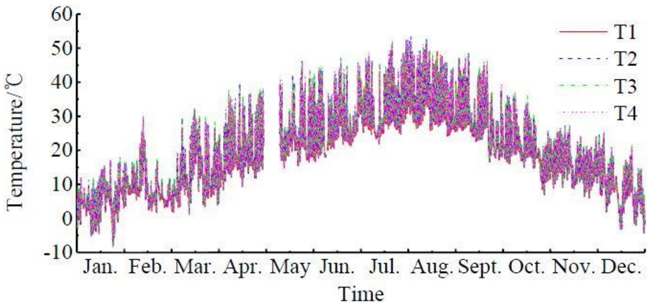

(a) The upper plate

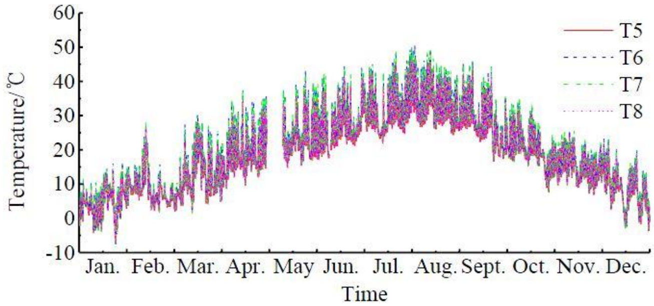

(b) The upper U rib

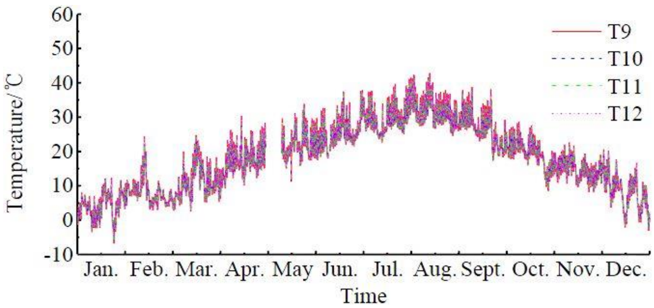

(c) The bottom U rib

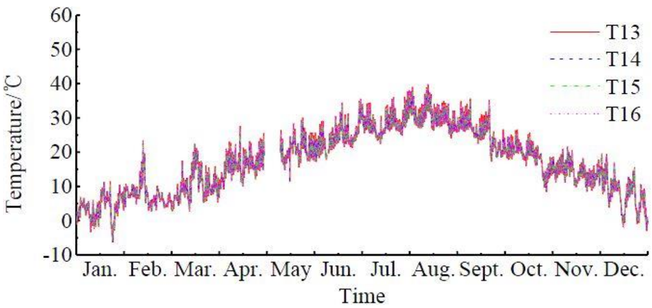

(d) The bottom plate

Fig. 4 Temperature variations of the flat steel-box girder

Table 1 The extreme values of the field temperature measurements (unit: °C)

Measurement point	Maximum	Minimum	Mean	Measurement point	Maximum	Minimum	Mean
T1	51.07	-7.92	19.89	T9	42.96	-6.61	18.51
T2	53.69	-8.87	20.47	T10	40.78	-5.86	18.33
T3	52.57	-8.76	20.53	T11	42.02	-6.64	18.30
T4	53.52	-8.11	19.90	T12	42.59	-6.42	18.44
T5	46.50	-7.40	19.02	T13	40.05	-6.29	17.57
T6	50.70	-8.04	20.23	T14	38.05	-5.63	17.47
T7	49.78	-8.28	20.07	T15	39.22	-6.07	17.47
T8	46.75	-7.29	19.17	T16	39.54	-5.83	17.60

As shown in Fig. 4, the temperatures at different measurement points present strong correlation. The maximum annual temperature difference on the steel box girder is slightly over 60 °C, which would make the main span expand by about 1 m, resulting in a large cumulative displacement of expansion joints. The extreme values of the field temperature measurements are listed in Table 1.

Table 1 indicates that the maximum temperature on this section decreases from the upper plate to the bottom plate vertically. However, the minimum temperature increases from top to bottom, with the lowest temperature on the upper plate and the highest temperature on the bottom plate. This is because sunlight directly irradiates the roof of the steel box girder in the daytime which generates heat, and that is transferred to the lower floor vertically. However, during nighttime, most heat comes from geothermal, and the air temperature at deck level is lower than ground level. The heat of the steel box girder is transferred from the inside to the air until the girder temperature becomes the same as the air temperature. Since the section of steel box girder is geometrically symmetrical along the central axis and the direction of the main girder is close to the North-South direction, the sunshine intensity on both sides of the steel box girder is similar around noon. The annual variation curve and extreme temperature at symmetrical measurement points about the central axis of the section are very close. In addition, there are also temperature differences across the cross section. The temperature of the upper measurement points close to the central axis is higher than that of the upper measurement points close to the sides. For example, the temperature of measurement points T2 and T3 are higher than that of measurement points T1 and T4. However, the opposite situation applies to the bottom measurement points. It shows that the thermal conductivity of the steel is far greater than that of the air. The heat transfer mode between the upper and lower surfaces of the steel box girder is mainly transmitted through the walls of the box girder, rather than the air inside the steel box girder.

In addition, distinct seasonal periodicity is obviously observed from the temperature variations. The temperature annual variation trend is similar to the sine curve (Xia *et al*. 2013, Xu *et al*. 2010). The lowest values of the temperature are recorded in January, while the highest values are recorded in July or August. The fitting formula of temperature variation trends is shown as follows

$$T = A \cdot sin\left(2\pi \cdot \frac{t}{365} + \theta\right) + B \tag{1}$$

where A represents the amplitude of the annual temperature variation. t represents the sampling time, and the unit of sampling time is day. θ and B represent the initial phase and the initial value, respectively. The parameters of the temperature variation trend at each measurement point are obtained based on the least square method (Gong 2000), as listed in Table 2. The comparison of the temperature variation trend at each measurement point is shown in Fig. 5.

Table 2 Fitting parameters of the annual temperature variation

Measurement point	A	B	θ	Measurement point	A	B	θ
T1	13.35	19.56	4.36	T9	12.44	18.19	4.31
T2	13.64	20.13	4.37	T10	11.91	17.97	4.29
T3	13.58	20.21	4.37	T11	11.93	17.98	4.29
T4	13.36	19.58	4.36	T12	12.38	18.12	4.31
T5	12.94	18.70	4.34	T13	11.96	17.26	4.29
T6	13.37	19.91	4.36	T14	11.67	17.14	4.28
T7	13.36	19.75	4.36	T15	11.87	17.16	4.28
T8	12.90	18.84	4.34	T16	11.88	17.28	4.29

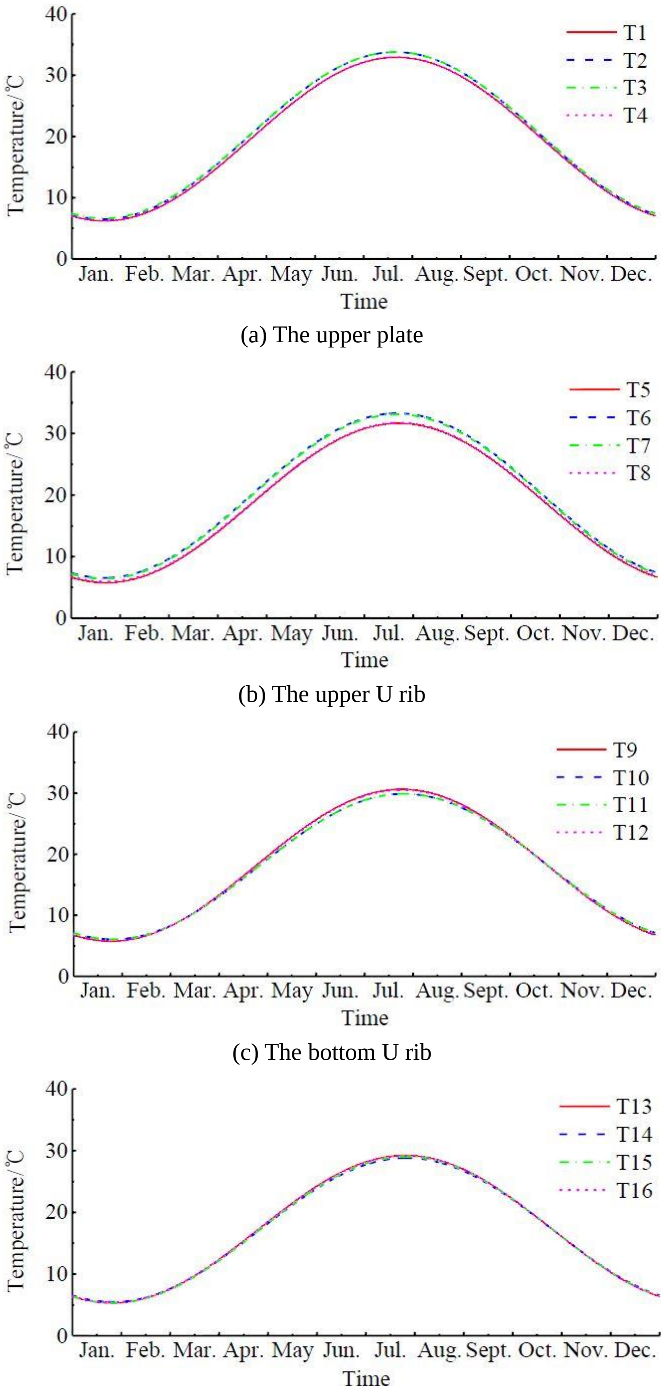

(a) The upper plate

(b) The upper U rib

(c) The bottom U rib

(d) The bottom plate

Fig. 5 The annual temperature variation trends

The initial phases of all the measurements are similar, indicating that all the annual temperature variations tend to be consistent. Meanwhile, the amplitude and the initial value of the upper measurement points are larger than that of the bottom measurement points, because the temperature of the upper measurement points is higher than that of the bottom measurement points. In addition, the comparison of the recorded temperature and annual temperature variation trends of measurement point T1 is illustrated in Fig. 6. The temperature variation without the annual variation trend is shown in Fig. 7. The annual temperature variation could be effectively removed from the field measurement using the Eq. (1). The daily temperature variation is clearly revealed. The daily temperature variation during Summer is the largest among the four seasons, which is around 25 °C, whlie during the Winter it is the smallest, which is around 10 °C.

Moreover, Fig. 4 shows that there is a distinct vertical temperature gradient in the section of the steel box girder. The average temperature and the extreme temperature of the upper plate are the highest, with those of the upper U rib the second and these of the bottom plate the lowest. This

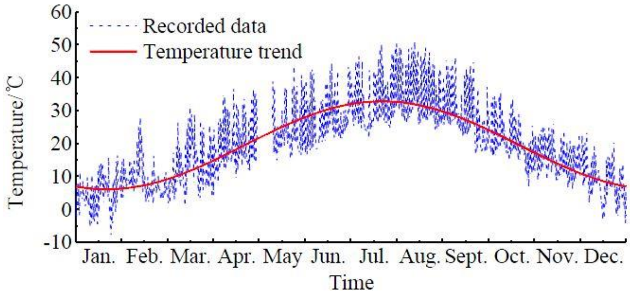

Fig. 6 The comparison of measured temperature trends at T1 points

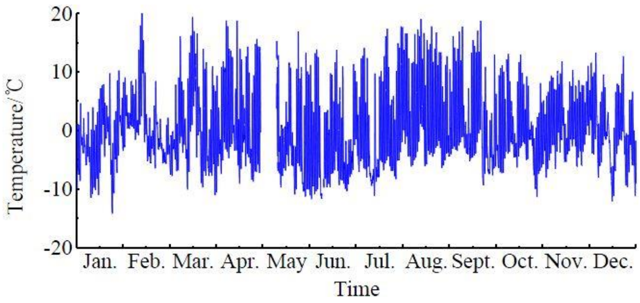

Fig. 7 The temperature variations without the seasonal trend

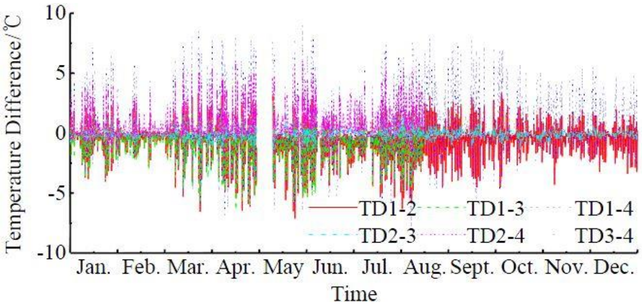

(a) The upper plate

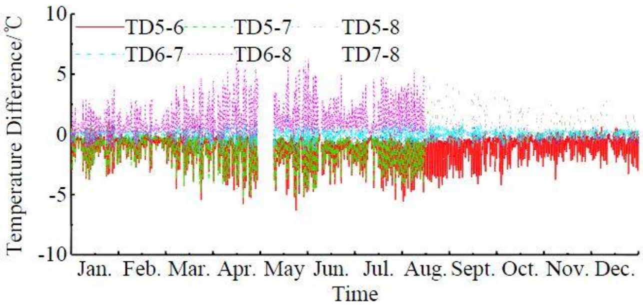

(b) The upper U rib

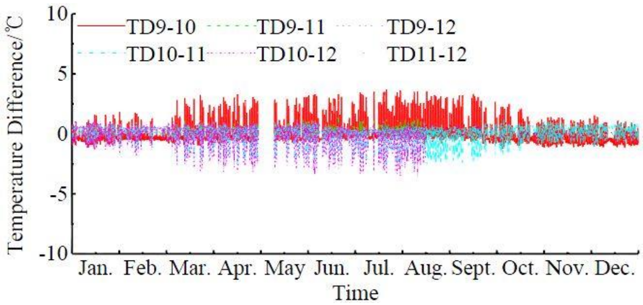

(c) The bottom U rib

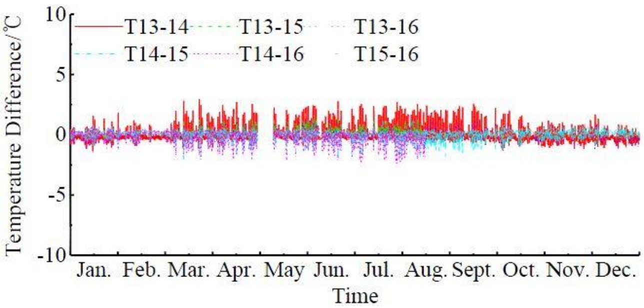

(d) The bottom plate

Fig. 8 Temperature difference variations on the flat steel-box girder in one year

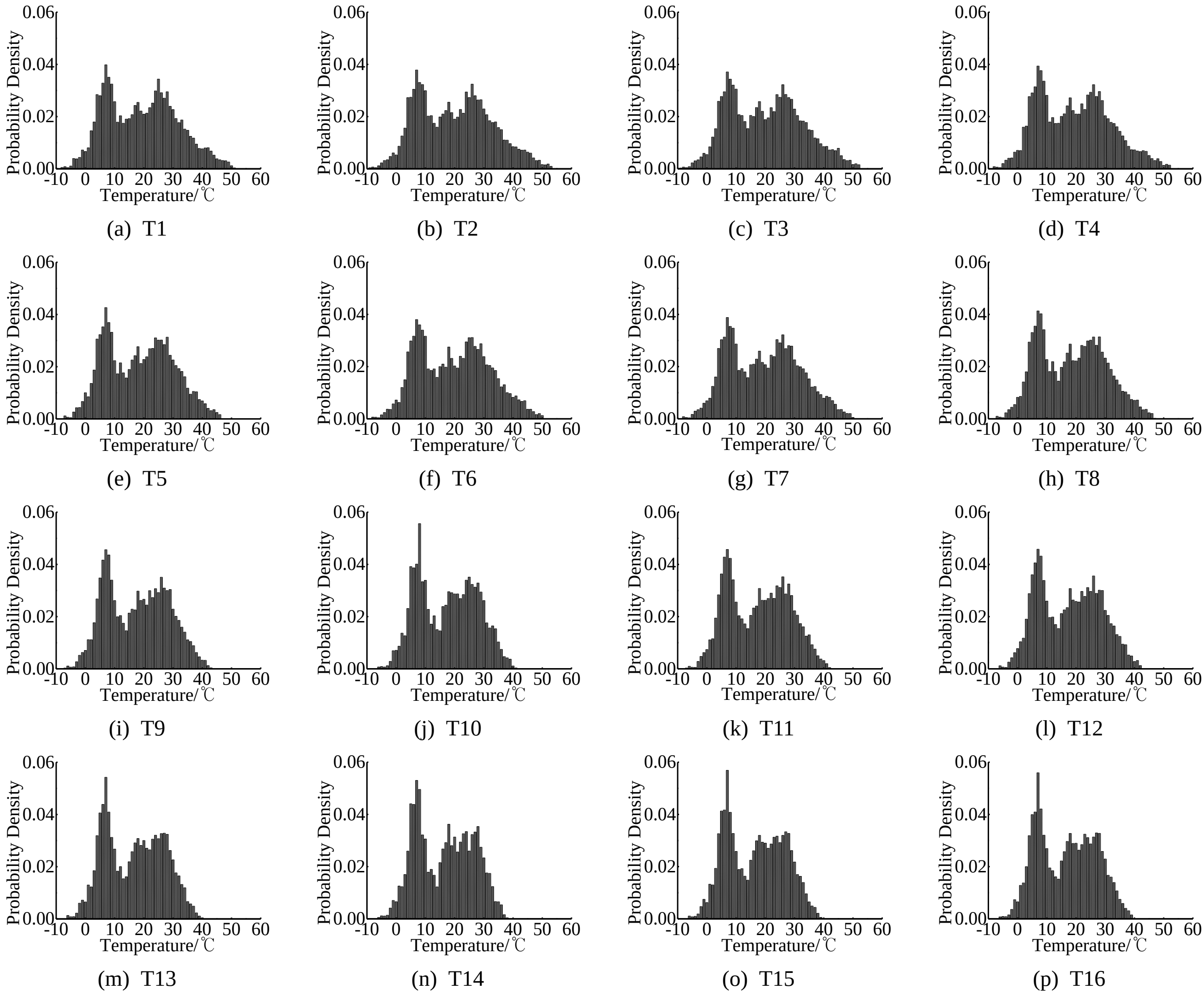

Fig. 9. Probability density distribution of temperature

is because the roof is directly subjected to solar radiation, and when the heat is conducted from the roof to the bottom through the diaphragm, the temperature gradually decreases.

Meanwhile, the horizontal temperature difference is investigated, which is calculated by

$$\mathrm{TD}i - j = \mathrm{T}i - \mathrm{T}j \qquad (2)$$

where TD*i*-*j* represents the temperature difference between the measurement point T*i* and T*j*. T*i* and T*j* represent the temperature of measurement points T*i* and T*j*, respectively. The calculations are shown in Fig. 8.

The temperature difference between the symmetrical measurement points is small while that between the asymmetrical measurement points is large. For example, the temperature difference TD3-4 is large for a set of asymmetric measurement points, while TD2-3 is small for a set of symmetric measurement points. It may be attributable to the following reasons: (1) the temperatures can be assumed uniform during the nighttime, since it is mainly influenced by the air temperature (Ding *et al*. 2012); and (2) the temperatures are mainly influenced by solar radiation during the daytime (Liu *et al*. 2012, Westgate *et al*. 2014). The section of the steel box girder of the SCB is geometrically symmetrical along the central axis. The direction of the main girder is close to the North-South direction and the solar intensity on both sides of the steel box girder is approximately identical around noon. In addition, the horizontal temperature gradient in the bottom plate is very small and can be ignored.

4. Probability density distributions of temperature and temperature difference

Statistical analysis is the best way to obtain rational probability distribution for a random variable (Mao *et al*. 2018). The field temperature measurements are employed to describe the statistical characteristics of temperature distribution in the flat steel box girder. The probability density distributions of one-year temperatures on the flat steel-box girder are shown in Fig. 9. Meanwhile, the probability density distributions of temperature differences

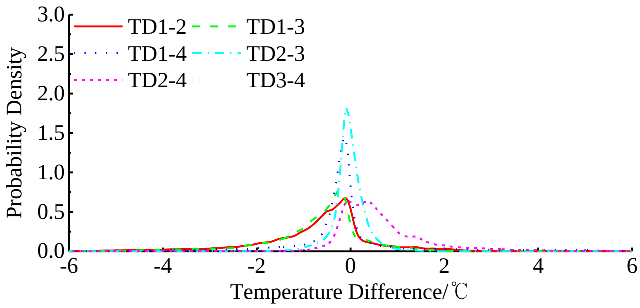

(a) The upper plate

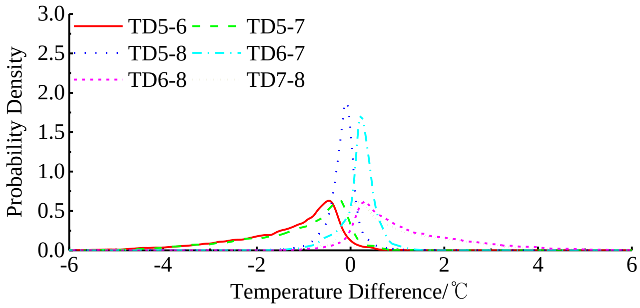

(b) The upper U rib

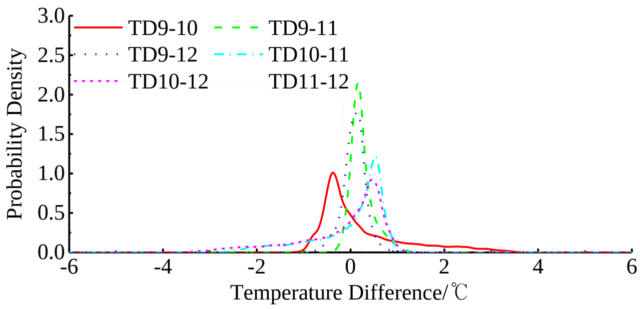

(c) The bottom U rib

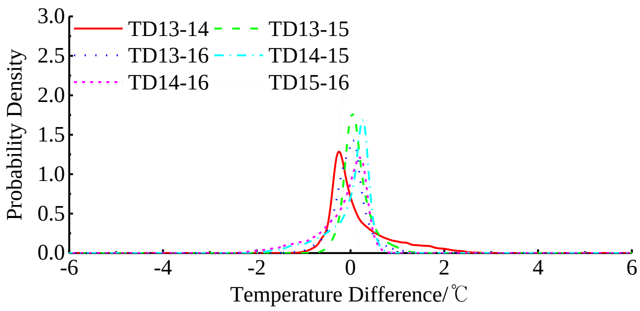

(d) The bottom plate

Fig. 10 Probability density distribution of temperature difference

are shown in Fig. 10.

As shown in Fig. 9, the peak positions of the probability density function at each measurement point are similar, approximately located at 7 °C, 17 °C and 26 °C, which indicate that the annual temperature variation trend at each measurement point is similar. In addition, on the steel box girder roof, especially on the upper plate, the peak value of probability density is relatively low and the position where the temperature exceeds 40 °C is relatively high, which indicates that the temperature distribution on the roof is more dispersed.

Skewness and kurtosis are often used to describe the shape characteristics of a distribution. Skewness is a measure of symmetry. Kurtosis is a measure of whether the data are heavy-tailed or light-tailed relative to a normal distribution (Groeneveld and Meeden 1984, Joanes and Gill 1998). The kurtosis and skewness of each measurement point are shown in Table 3. The formulas for calculating kurtosis (γ_4) and skewness (γ_3) are as follows

$$\gamma_3 = E\left[\left(\frac{u(x)-\mu}{\sigma}\right)^3\right] \tag{3}$$

Table 3 The calculations of kurtosis and skewness

Measurement point	Skewness	Kurtosis	Measurement point	Skewness	Kurtosis
TD1-2	-0.7766	2.6904	TD9-10	1.4403	1.6253
TD1-3	-1.2935	3.7589	TD9-11	1.2036	2.2964
TD1-4	1.3033	6.2198	TD9-12	-0.3614	1.0032
TD2-3	-0.6266	3.8234	TD10-11	-1.4179	1.4606
TD2-4	1.7355	4.4418	TD10-12	-1.3958	1.5199
TD3-4	2.2090	6.6854	TD11-12	-1.1556	1.7134
TD5-6	-1.1208	0.8986	TD13-14	1.4843	2.2972
TD5-7	-1.0678	0.6006	TD13-15	0.9181	2.3667
TD5-8	0.4584	5.5257	TD13-16	0.01044	1.7264
TD6-7	-1.1612	2.5525	TD14-15	-1.5871	2.6327
TD6-8	1.1840	1.1999	TD14-16	-1.4167	2.2841
TD7-8	1.3316	1.7518	TD15-16	-1.1380	3.0178

$$\gamma_4 = E\left[\left(\frac{u(x)-\mu}{\sigma}\right)^4\right] - 3 \tag{4}$$

where E[*] represents the expectation calculation. μ and σ represent the mean value and variance of the variable, respectively.

Fig. 10 indicates that the temperature difference distribution does not follow the Gaussian distribution. In fact, it is non-Gaussian with high skewness among the measurement points which are asymmetrically arranged on the section and high kurtosis which are symmetrically nged. The kurtosis of temperature difference on the bottom plate is larger than that of other measurement points, arra since there is no solar radiation on the bottom plate, the temperature distribution of bottom plate is more uniform.

5. The general formula of the probability density distribution

The weighted sum of four Normal distributions is selected to describe the probability density distribution of temperature, as follows

$$\begin{aligned} f(T) = {} & \frac{a_1}{\sigma_1\sqrt{2\pi}} e^{-\frac{(T-\mu_1)^2}{2\sigma_1^2}} + \frac{a_4}{\sigma_4\sqrt{2\pi}} e^{-\frac{(T-\mu_2)^2}{2\sigma_2^2}} \\ & + \frac{a_3}{\sigma_3\sqrt{2\pi}} e^{-\frac{(T-\mu_3)^2}{2\sigma_3^2}} + \frac{a_4}{\sigma_4\sqrt{2\pi}} e^{-\frac{(T-\mu_4)^2}{2\sigma_4^2}} \end{aligned} \tag{5}$$

where a_1, a_2, a_3 and a_4 represent the weight of the Normal distributions, respectively. μ_1, δ_1, μ_2, δ_2, μ_3, δ_3, μ_4 and δ_4 represent the parameters of the Normal distributions,

Table 4 Fitting parameters of the probability density distribution of temperature

Measurement point	a_1	μ_1	σ_1	a_1	μ_2	σ_2	a_1	μ_3	σ_3	a_1	μ_4	σ_4
T1	0.3684	6.79	3.51	0.1131	16.49	2.49	0.3921	25.15	4.90	0.1265	35.22	5.14
T2	0.3500	6.94	3.62	0.1110	16.93	2.51	0.1232	25.16	2.96	0.4158	29.10	8.60
T3	0.2851	6.99	3.48	0.0400	17.16	1.66	0.0679	26.22	2.58	0.6069	26.22	11.05
T4	0.3575	7.39	3.61	0.1124	17.14	2.40	0.1524	25.25	3.50	0.3777	30.54	7.96
T5	0.3622	7.49	3.87	0.1013	17.22	2.15	0.1740	25.47	3.65	0.3625	31.39	8.72
T6	0.3636	7.27	3.67	0.1140	16.84	2.30	0.2411	25.01	4.11	0.2814	32.69	7.28
T7	0.3578	7.11	3.59	0.1175	17.16	2.43	0.1526	25.60	3.33	0.3721	29.60	8.86
T8	0.3685	6.92	3.49	0.0960	16.60	2.31	0.4647	25.70	5.58	0.0708	38.09	4.24
T9	0.3830	6.63	2.99	0.1842	16.95	2.94	0.4277	26.07	4.84	0.0051	33.79	0.57
T10	0.3673	6.91	3.12	0.2007	17.42	3.30	0.3714	26.50	4.28	0.0606	35.55	3.07
T11	0.3513	6.90	2.82	0.1872	17.44	2.87	0.3797	26.41	4.56	0.0818	35.32	12.78
T12	0.3946	7.39	3.23	0.1320	17.54	2.53	0.4571	26.00	4.99	0.0163	34.25	1.09
T13	0.3867	6.62	3.01	0.2252	17.39	3.11	0.3657	26.29	4.15	0.0223	34.08	2.09
T14	0.3737	6.81	3.16	0.2014	17.42	3.20	0.3611	26.27	4.13	0.0638	34.87	2.95
T15	0.3734	6.85	3.19	0.1737	17.16	3.06	0.4000	26.19	4.62	0.0529	35.66	2.98
T16	0.3910	6.69	3.10	0.1913	17.20	2.86	0.3996	26.06	4.57	0.0181	34.67	2.03

Table 5 Fitting parameters of the probability density distribution of temperature difference

Measurement point	b_1	k	λ	t	c	b_2	μ	σ
TD1-2	0.60	8.27	9.18	8.11	-1	0.40	0.60	0.28
TD1-3	0.64	4.49	4.18	3.20	-1	0.36	0.64	0.24
TD1-4	0.56	45.74	6.24	-6.38	1	0.44	0.56	1.65
TD2-3	0.55	13.26	1.51	1.43	-1	0.45	0.55	0.39
TD2-4	0.50	2.60	2.04	-0.97	1	0.50	0.50	0.33
TD3-4	0.52	2.48	2.03	-0.99	1	0.48	0.52	0.26
TD5-6	0.71	2.04	2.23	0.53	-1	0.29	0.71	0.26
TD5-7	0.72	1.96	2.28	0.71	-1	0.28	0.72	0.25
TD5-8	0.60	7.55	2.00	1.71	-1	0.40	0.60	0.10
TD6-7	0.55	22.50	2.58	2.80	-1	0.45	0.55	0.45
TD6-8	0.70	2.17	2.45	-0.89	1	0.30	0.70	0.27
TD7-8	0.68	2.12	2.42	-0.99	1	0.32	0.68	0.27
TD9-10	0.67	1.54	1.68	-1.09	1	0.33	0.67	0.23
TD9-11	0.69	1.86	0.54	-0.25	1	0.31	0.69	0.08
TD9-12	0.11	10.77	0.68	0.87	-1	0.89	0.11	0.22
TD10-11	0.65	1.60	1.40	1.05	-1	0.35	0.65	0.18
TD10-12	0.64	1.75	1.81	1.23	-1	0.36	0.64	0.23
TD11-12	0.66	2.32	0.47	0.23	-1	0.34	0.66	0.06
TD13-14	0.61	2.13	1.51	-1.07	1	0.39	0.61	0.16
TD13-15	0.52	2.61	0.94	-0.67	1	0.48	0.52	0.14
TD13-16	0.78	6.13	1.94	1.77	-1	0.22	0.78	0.12
TD14-15	0.60	1.99	0.99	0.75	-1	0.40	0.60	0.11
TD14-16	0.62	2.19	1.16	0.77	-1	0.38	0.62	0.17
TD15-16	0.62	2.19	1.16	0.77	-1	0.38	0.62	0.17

respectively.

Meanwhile, the weighted sum of Weibull distribution and the Normal distribution is selected to describe the probability density distribution of temperature difference, as follows

$$f(TD) = b_1 \cdot \frac{k}{\lambda}\left(\frac{TD-t}{c\cdot\lambda}\right)^{k-1} e^{-\left(\frac{TD-t}{c\cdot\lambda}\right)^k} + \frac{b_2}{\delta\sqrt{2\pi}} e^{-\left(\frac{TD-\mu}{2\sigma^2}\right)^k} \quad (6)$$

where b_1 and b_2 represent the weight of the Weibull distribution and the Normal distribution, respectively. k and λ represent the parameters of the Weibull distribution. μ and δ represent the parameters of the Normal distribution. c is equal to 1 or -1. t represent the threshold of the temperature difference.

Based on the field monitoring data, the fitting parameters of the joint probability density functions are obtained based on the least square method (Gong 2000). The fitting parameters of temperature and temperature difference are listed in Tables 4 and 5, respectively.

The fitted and measured probability density distributions of the temperature are displayed in Fig. 11. Meanwhile, the fitted and measured probability density distributions of the temperature difference are displayed in Fig. 12. Figs. 11 and 12 indicate that the probability density functions of temperature and temperature difference can be accurately

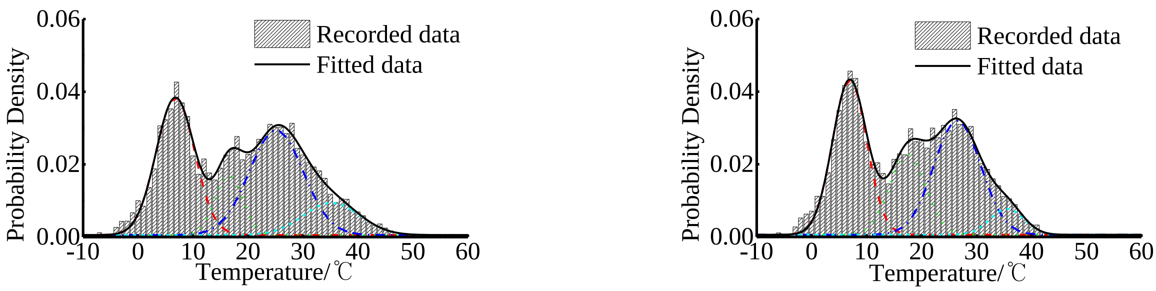

(a) T5 (b) T9

Fig. 11 Comparison between the fitted and measured probability density of temperature

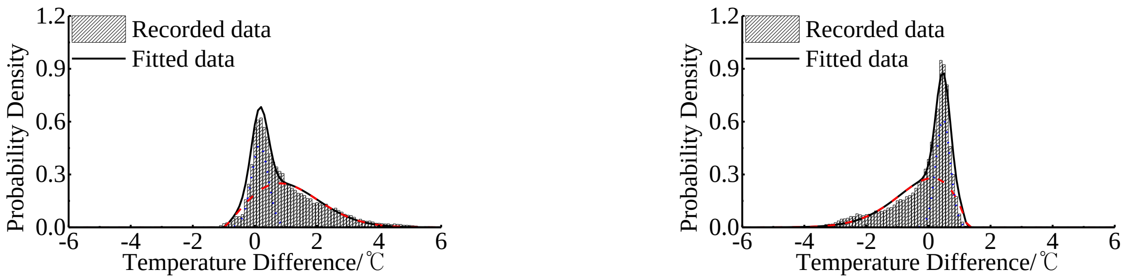

(a) TD7-8 (b) TD10-12

Fig. 12 Comparison between the fitted and measured probability density of temperature difference

described by the general formulas. Hence, the results can provide reliable references for the consideration of temperature effect in the design and maintenance of long-span cable-stayed bridges.

6. Conclusions

Comprehensive understanding of temperature distributions provides reliable references for structural design and performance evaluation of bridges. The temperature distribution of the steel box girder is systematically investigated based on the field monitoring data of the SCB. Accordingly, the general formulas are proposed to describe the probability density distribution of the temperature and temperature difference. The following conclusions can be drawn from this study:

- Seasonal periodicity is observed from the temperature on the flat steel-box girder. The annual temperature variation trend is fairly similar to the sine curve. The lowest values of the temperature are recorded in January, while the highest values are recorded in July or August. In addition, the temperature at different measurement points presents strong correlation.
- The annual temperature variation trend at all the measurement points on the steel box girder is similar. Meanwhile, the peak positions of the probability density distribution at all measurement points are similar.
- The temperature difference distribution for the asymmetrically arranged measurement points present evident non-Gaussianity. The skewness of the asymmetrically arranged measurement points is higher than that of symmetrically arranged measurement points. However, the kurtosis of symmetrical arrangement points is higher than that of asymmetrical arrangement points.
- The probability density distributions of the temperature and temperature difference can be described with general formulas. Specifically, the probability density distribution of temperature can be described with a weighted sum of four Normal distributions, while that of the temperature difference can be described with a weighted sum of a Weibull distribution and a Normal distribution.

Acknowledgments

The authors would like to gratefully acknowledge the supports from the National Basic Research Program of China (973 Program) (Grant No. 2015CB060000), the National Natural Science Foundation of China (Grant No. 51722804), the National Ten Thousand Talent Program for Young Top-notch Talents (Grant No. W03070080), the Jiangsu Transportation Scientific Research Project (Grant No. 8505001498), the Jiangsu Key R & D Plan (Grant No. BE2018120), and the Postgraduate Research & Practice Innovation Program of Jiangsu Province (Grant No. KYCX19_0095). The authors also thank the help from Jiangsu Transportation Institute (JSTI) for providing long-term monitoring data.

References

Ding, Y.L., Zhou, G.D., Li, A.Q. and Wang, G.X. (2012), "Thermal field characteristic analysis of steel box girder based on long-term measurement data", *Int. J. Steel Struct.*, **12**(2), 219-232.

Gong, J. (2000), "A new probability index for estimating Weibull modulus for ceramics with the least-square method", *J. Mater. Sci. Lett.*, **19**(10), 827-829. https://doi.org/10.1023/A:1006712809728

Groeneveld, R.A. and Meeden, G. (1984), "Measuring skewness and kurtosis", *J. Royal Statist. Soc.: Series D* (*The Statistician*), **33**(4), 391-399. https://doi.org/10.2307/2987742

Guo, T., Liu, J., Zhang, Y. and Pan, S. (2014), "Displacement monitoring and analysis of expansion joints of long-span steel bridges with viscous dampers", *J. Bridge Eng.*, **20**(9), 04014099. https://doi.org/10.1061/(ASCE)BE.1943-5592.0000701

Ho, D. and Liu, C.H. (1989), "Extreme thermal loadings in highway bridges", *J. Struct. Eng.*, **115**(7), 1681-1696. https://doi.org/10.1061/(ASCE)0733-9445(1989)115:7(1681)

Im, C.K. and Chang, S.P. (2004), "Estimating extreme thermal loads in composite bridge using long-term measured data", *Int. J. Steel Struct.*, **4**(1), 25-31.

Joanes, D.N. and Gill, C.A. (1998), "Comparing measures of sample skewness and kurtosis", *J. Royal Statist. Soc.: Series D* (*The Statistician*), **47**(1), 183-189. https://doi.org/10.1111/1467-9884.00122

Liu, H.B., Chen, Z.H. and Zhou, T. (2012), "Theoretical and experimental study on the temperature distribution of H-shaped steel members under solar radiation", *Appl. Thermal Eng.*, **37**, 329-335. https://doi.org/10.1016/j.applthermaleng.2011.11.045

Macdonald, J.H. and Daniell, W.E. (2005), "Variation of modal parameters of a cable-stayed bridge identified from ambient vibration measurements and FE modelling", *Eng. Struct.*, **27**(13), 1916-1930. https://doi.org/10.1016/j.engstruct.2005.06.007

Mao, J.X., Wang, H., Feng, D.M., Tao, T.Y. and Zheng, W.Z. (2018), "Investigation of dynamic properties of long-span cable-stayed bridges based on one-year monitoring data under normal operating condition", *Struct. Control Health Monitor.*, **25**(5), e2146. https://doi.org/10.1002/stc.2146

Saetta, A., Scotta, R. and Vitaliani, R. (1995), "Stress analysis of concrete structures subjected to variable thermal loads", *J. Struct. Eng.*, **121**(3), 446-457. https://doi.org/10.1061/(ASCE)0733-9445(1995)121:3(446)

Salawu, O.S. (1997), "Detection of structural damage through changes in frequency: a review", *Eng. Struct.*, **19**(9), 718-723. https://doi.org/10.1016/S0141-0296(96)00149-6

Spencer Jr, B.F., Ruiz, M.E. and Kurata, N. (2004), "Smart sensing technology: opportunities and challenges", *Struct. Control Health Monitor.*, **11**(4), 349-368. https://doi.org/10.1002/stc.48

Tong, M., Tham, L.G., Au, F.T.K. and Lee, P.K.K. (2001), "Numerical modelling for temperature distribution in steel bridges", *Comput. Struct.*, **79**(6), 583-593. https://doi.org/10.1016/S0045-7949(00)00161-9

Wang, H., Tao, T.Y., Li, A.Q. and Zhang, Y.F. (2016), "Structural health monitoring system for Sutong cable-stayed bridge", *Smart Struct. Syst., Int. J.*, **18**(2), 317-334. https://doi.org/10.12989/sss.2016.18.2.317

Westgate, R., Koo, K.Y. and Brownjohn, J. (2014), "Effect of solar radiation on suspension bridge performance", *J. Bridge Eng.*, **20**(5), 04014077. https://doi.org/10.1061/(ASCE)BE.1943-5592.0000668

Xia, Y., Xu, Y.L., Wei, Z.L., Zhu, H.P. and Zhou, X.Q. (2011), "Variation of structural vibration characteristics versus non-uniform temperature distribution", *Eng. Struct.*, **33**(1), 146-153. https://doi.org/10.1016/j.engstruct.2010.09.027

Xia, Y., Chen, B., Zhou, X.Q. and Xu, Y.L. (2013), "Field monitoring and numerical analysis of Tsing Ma Suspension Bridge temperature behavior", *Struct. Control Health Monitor.*, **20**(4), 560-575. https://doi.org/10.1002/stc.515

Xia, Q., Zhang, J., Tian, Y.D. and Zhang, Y.F. (2017), "Experimental study of thermal effects on a long-span suspension bridge", *J. Bridge Eng.*, **22**(7), 04017034. https://doi.org/10.1061/(ASCE)BE.1943-5592.0001083

Xu, Y.L., Chen, B., Ng, C.L., Wong, K.Y. and Chan, W.Y. (2010), "Monitoring temperature effect on a long suspension bridge", *Struct. Control Health Monitor.*, **17**(6), 632-653. https://doi.org/10.1002/stc.340

Yarnold, M.T. and Moon, F.L. (2015), "Temperature-based structural health monitoring baseline for long-span bridges", *Eng. Struct.*, **86**, 157-167. https://doi.org/10.1016/j.engstruct.2014.12.042

Ye, J.S., Lei, X. and Wang, Y. (2009), "Study of Characteristic Value of Thermal Difference of Concrete Box Girder Based on Statistical Analysis", *J. Highway Transport. Res. Develop.*, **26**(11), 50-54.

Zhang, X.G., Pei, M.S., Yuan, H., Xu, L.P. and Zhu, B. (2009), "Study on structural system of Sutong Bridge", *Eng. Sci.*, **11**(3), 20-25.

Zhang, X.G., Liu, G., Ma, J., Wu, H., Fu, B. and Gao, Y. (2015), "Status and prospect of technical development for bridges in China", *Chinese Sci. Bull.*, **61**(4-5), 415-425.

Zhou, G.D., Ding, Y.L., Li, A.Q. and Wang, G.X. (2012), "Thermal difference characteristic analysis of a flat steel box girder in long-span suspension bridge based on long-term field measurement data", *China Civil Eng. J.*, **1**(5), 114-125.

Zuk, W. (1965), "Thermal behavior of composite bridges-insulated and uninsulated", *Highway Res. Record*, **76**, 231-253.

BS